Clean Technologies and Environmental Policy (2024) 26:1965–1974
https://doi.org/10.1007/s10098-023-02721-x

ORIGINAL PAPER

Valorization of waste glass from discarded fluorescent lamps as additional active material in the synthesis of alkali-activated materials

Nicolaie Marin[1] · Cristina Orbeci[1] · Liliana Bobirică[1] · Luoana Florentina Pascu[2] · Constantin Bobirică[1]

Received: 10 July 2023 / Accepted: 26 December 2023 / Published online: 16 February 2024

Abstract

Currently, the hazardous potential of spent fluorescent lamps due to their mercury content, which usually exceeds the limit allowed by standards, it is well known. When these are taken out from use, mercury is distributed between all the components of the lamp; in particular, it can be found in the phosphorescent powder called "phosphor" which is attached as a thin layer on the walls of the lamps. Although many efforts have been made to develop technologies for recovery of mercury, in many cases their effectiveness is very hard to be proved from both technical and economic points of view. Therefore, this work is focused on evaluating the feasibility of valorizing this type of waste glass as an active precursor for the synthesis of fly ash-based alkali-activated materials. In this respect, the potential of synthesized alkali-activated materials to immobilize mercury from waste glass added to the synthesis mixture was experimentally proved through compliance leaching tests. Important microstructural changes that appear with the increasing addition of waste glass to the synthesis mixture were highlighted by SEM and N_2-BET analysis. Sharp increase in the SiO_2/Al_2O_3 molar ratio of the synthesis mixture with the increasing addition of waste glass leads to an increase in the unreacted glassy fraction that acts as defect sites in the structure of the alkali-activated material, having a negative effect on its mechanical properties. However, the compressive strength tests showed that an addition of waste glass up to 5% of the total mass of the synthesis mixture has a beneficial effect on the compressive strength of alkali-activated materials.

Graphical abstract

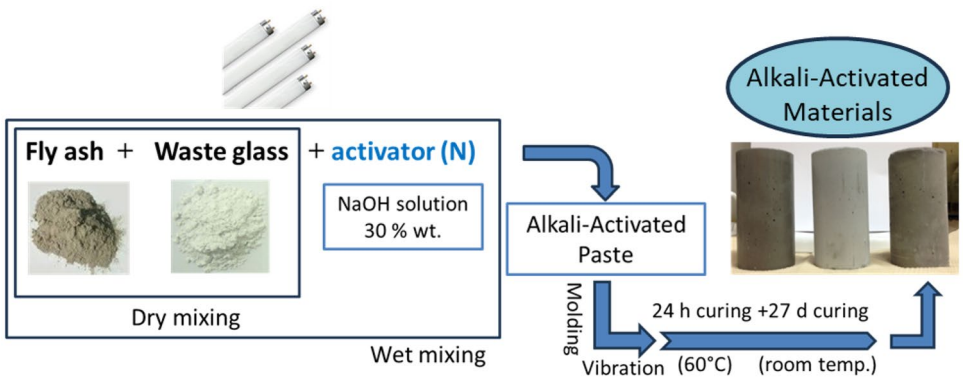

Schematic diagram for the manufacture of alkali-activated materials

Keywords Fluorescent lamps · Fly ash · Alkali-activated materials · Mercury · Waste glass

Extended author information available on the last page of the article

Introduction

The wastes derived from the lighting equipment, and especially those related to fluorescent lamps, are often classified as hazardous because of their hazardous components such as mercury (US EPA 1997). At the time of their removal from use, a part of mercury added during manufacture is still present in vapor phase in the lamp, but the largest part of it is adsorbed on the components of the lamp, namely on the glass, end caps and fluorescent powder (Rey-Raap and Gallardo 2012). Although a wide range of treatment technologies have been developed to remove and recover the mercury followed by the valorization of the components of the lamps, in many cases their effectiveness is difficult to prove from both technical and economic standpoints (Li et al. 2023).

The waste glass both non-hazardous and hazardous, such as cathode ray tubes (CRTs) waste glass containing lead, has been often used in cement-based mortars and concretes to replace the natural aggregate with good results (Hama et al. 2023). However, because the glass is unstable under alkaline conditions of the cement-based materials, some deleterious effects were reported due to alkali–silica reaction (Liu et al. 2022). The alkali–silica gel which is forming expands in the presence of water and leads to the cracking of the material making it more vulnerable to the aggressive agents in the environment (Abbas 2023).

Alkali-activated aluminosilicate-based materials could be an attractive alternative to cement-based materials because of their characteristics such as high strength and durability in different aggressive environments, low cost and other environmental benefits related to the raw materials which can be used (Occhicone et al. 2022; Ricciotti et al. 2023). Basically, the alkali activation mechanism involves the dissolution, condensation and polymerization in alkaline media of aluminum and silica precursors derived from the glassy alumino-silicate phases that are present in the raw materials both natural and treated aluminosilicates or in the secondary raw materials such as fly ash, bottom ash, ground granulated blast furnace slag, phosphogypsum, silica fume, red mud, mine tailings, waste glass and even some ash from agriculture (i.e., rice husk ash, bagasse ash, palm oil fuel ash, etc.) (Frasson and Rocha 2023).

As other precursors for the synthesis of alkali-activated materials, the glass powder is an aluminosilicate material rich in silica and could be also used for alkali-activated materials production (Çelik et al. 2023). Both sodium silicate hydrate (N-S-H) gel and sodium aluminosilicate hydrate (N-A-S-H) gel are formed when a mixture of glass powder and fly ash is activated with an alkaline solution (hydroxide or silicate solutions) leading to the formation of an alkali-activated material with proper mechanical characteristics (Özkılıç et al. 2023). A series of studies were performed related to the use of waste glass (non-hazardous or hazardous waste glass) to produce alkali-activated materials. In this respect, it was established that to obtain good results in terms of both mechanical and leaching properties a special attention must be given to the choosing of mixture composition with an emphasis on establishing optimal molar ratios between the main oxides of the system such as SiO_2/Al_2O_3, M_2O/SiO_2, M_2O/Al_2O_3, H_2O/M_2O (M is Na or K), as well as to establish the optimal reaction conditions such as curing temperature, curing time, alkali concentration, liquid/solid ratio (Komnitsas and Zaharaki 2007). It should be noted that damages induced by the alkali silica reaction due to addition of reactive silica such as waste glass are significantly lower in alkali-activated materials compared to cement-based materials (Lei et al. 2020).

Besides the positive effects that has the addition of waste glass to the mixture, its hazardous constituents could be successfully immobilized in the structure of the final product (Long et al. 2021). The efficiency with which contaminants are immobilized in the alkali-activated material largely depends on its microstructure (total porosity, pore shape and pore size distribution), as well as on its phase composition (Zhang et al. 2008). The main mechanisms of contaminant immobilization are physical encapsulation, sorption, precipitation and chemical bonding in the three-dimensional aluminosilicate structure of the alkali-activated material (Tian et al. 2022).

Therefore, the aim of this work is to explore the feasibility of using the waste glass containing mercury, from discarded fluorescent lamps, as an active component of the alkali-activated system to produce fly ash/waste glass-based alkali-activated materials that meet the required properties that allow them to be environmental-friendly and valorized in the construction field.

Materials and methods

Materials

A class F fly ash of coal origin was obtained from a power plant and was used as raw material to prepare all the alkali-activated mixtures. The waste glass comes from the discarded fluorescent tubes which were obtained from one of the collection points. The lamps used in the experiments (40 units) were of the same type and same brand (FL20SD/18). The glass derived from these lamps is coated inside with a thin layer of fluorescent powder generically called "phosphor" and was added to the system in powder form to replace

the fly ash in different proportions. In this respect, the glass was manually crushed into a controlled crushing system, and then, it was ground in a ball mill until a fine powder was obtained (particles less than 74 µm). The oxide composition together with other chemical and physical properties of the powdered raw materials is presented in Table 1. The technical characteristics of the spent fluorescent lamps are presented in Table 2. A sodium hydroxide (analytical grade) solution of 30% (by mass) was prepared and used as activator for all synthesis mixtures. Glacial acetic acid (analytical grade) was used to prepare the leaching solution for the leaching tests. Deionized water was used throughout all experiments.

For a safe operation, a crushing system was designed to allow mercury vapor recovery from inside of the fluorescent tubes. In this respect, each fluorescent lamp was introduced in a braid reinforced polyvinylchloride (PVC) hose. One of the PVC hose's ends was connected through a polypropylene (PP) hose to a vessel containing a mixture of nitric acid and hydrochloric acid (5% each by volume). It should be noted that the connection was perfectly sealed to prevent mercury vapor from escaping. The other end of the PVC hose is provided with a rubber plug that allows (by intermittently disconnecting it) the introduction of new fluorescent lamps to be broken by repeated blows with a hammer. The mercury vapor released in the PVC hose is drawn into the vessel containing the acid mixture with the help of a peristaltic pump connected to it through a PP hose. The peristaltic pump is

Table 2 Technical characteristics of the spent fluorescent lamps

Type	Model name	Nominal wattage, W	Dimensions, mm	
			Tube diameter	Total length
Starter type	FL20SD/18	18	28 ± 1.5	580 ± 1.5

Table 1 Chemical and physical characteristics of the raw materials. The oxide composition was determined by XRF analysis, and the mercury content was determined according to the standard procedure method 7471B

	Fly ash (FA)	Waste glass (WG)
Oxide	% (by mass)	
SiO_2	54.77	58.39
Al_2O_3	21.04	1.92
CaO	9.57	11.69
Fe_2O_3	6.74	0.16
SO_3	1.72	0.13
MgO	1.37	2.6
K_2O	1.36	1.04
TiO_2	1.17	0.06
Na_2O	0.94	15.3
P_2O_5	0.86	7.85
BaO	0.15	0.11
SrO	0.12	0.06
MnO	0.07	0.08
ZrO_2	0.06	0.04
ZnO	0.03	–
CuO	0.02	–
NiO	0.01	–
Rb_2O	0.01	–
Sb_2O_3	–	0.32
PbO	–	0.19
Cl	–	0.07
Y_2O_3	–	0.03
Mercury content	mg/kg of dry material	
Hg	0.34	4
Surface area	m^2/g	
BET (Brunauer–Emmett–Teller) method	4.46	0.47
Total pore volume	cm^3/g	
BJH (Barrett–Joyner–Halenda) method	4.24×10^{-3}	1.60×10^{-3}
Average pore diameter	nm	
BJH method	3.44	3.81

set before the start of the breaking operation at maximum speed and to operate for 10 min. Finally, the end caps of the fluorescent tube are removed, and the glass cullet is ground in a ball mill.

Sample preparation

Five different alkali-activated mixtures were prepared by replacing the fly ash with different proportions of waste glass, namely 0, 5, 10, 15 and 25% (by mass). A detailed description of these mixtures is presented in Table 3. All the samples were prepared at the same water/solid mass ratio (w/s) of 0.35. Thus, the fly ash was dry mixed by hand with the glass powder (except for FA-N-0 mixture) for 10 min and then with the activator solution for other 10 min. The resulting paste was molded into 5 cm (d) × 10 cm (h) cylindrical polypropylene (PP) formworks and then vibrated for 2 min. The formworks were sealed in plastic bags and kept at 60 °C for 24 h. Next, the samples were kept for another 24 h at 20 °C and then de-molded, sealed again and cured for another 26 days at 20 °C. Three replicates were prepared for each alkali-activated mixture.

Analysis and test methods

After 28 days of curing, the specimens (alkali-activated materials) were subjected to a series of tests to characterize them from both physical and chemical standpoints. In this respect, the alkali-activated materials were tested for their compressive strength according to ASTM C39/C39M-14 standard and for their hazardous potential related to mercury (along with the raw materials from which they were prepared) according to toxicity characteristic leaching procedure (TCLP)/method 1311. The analysis of mercury in the raw materials, as well as the analysis of mercury in the leachates, was determined according to the standard procedure for determination of mercury in solid or semisolid waste (method 7471B) and using an atomic absorption spectrometer type contrAA-300. The composition of the raw materials (Table 1) was determined by X-ray fluorescence (XRF) on a Bruker-AXS S4 Pioneer spectrophotometer. Nitrogen adsorption–desorption isotherms of both raw materials and alkali-activated materials were measured on an Autosorb IQ MP Physisorption Analyser at 77.35 K. From the isotherms data and by using the Brunauer–Emmett–Teller (BET) method, the specific surface area was calculated. Cumulative pore volume and pore size distribution were determined from the desorption data and by using the Barrett–Joyner–Halenda (BJH) method. Powder X-ray diffraction was performed on a Bruker-AXS D5005 diffractometer using CuKα radiation ($\lambda = 1.5406$ nm) over a scanning range of 5–90° (2θ) at 40 kV (operating voltage), 30 mA (current) and a scanning rate of 1°/min. The crystalline phases were identified by using the JCPDS reference. Zeiss SUPRA 55-VP scanning electron microscope (SEM) equipped with energy-dispersive spectroscopy (EDX) analyzer (operated at 15.0 kV) was used for morphological observations, as well as for elemental analysis. Samples were prepared for platinum coating by using a Bal-Tec SCD005 sputter coater.

Table 3 Composition of the alkali-activated mixtures

Component, % (by mass)					
Mixture	FA-N-0	FA-N-5	FA-N-10	FA-N-15	FA-N-25
Fly ash	66.67	61.67	56.67	51.67	41.67
Waste glass	0	5	10	15	25
Na_2O (from activator)	7.75	7.75	7.75	7.75	7.75
Water (from activator)	25.58	25.58	25.58	25.58	25.58
Total	100	100	100	100	100
Molar ratios					
$^*M_2O/SiO_2$	0.23	0.25	0.268	0.285	0.319
Si_2O/Al_2O_3	4.417	4.764	5.165	5.635	6.866
H_2O/M_2O	10.05	9.296	8.647	8.083	7.15
M_2O/Al_2O_3	1.028	1.193	1.383	1.607	2.192
Mass ratio					
Na_2O/powder	0.116	0.116	0.116	0.116	0.116

$^*M_2O$–Na_2O and K_2O from fly ash, waste glass and activator

Results and discussion

As it was expected for this type of waste, the compliance leaching tests (TCLP) confirmed their hazardous characteristics in relation to the mercury content. The concentration of mercury in the leachate, as shown in Fig. 1, is almost two times higher than the maximum concentration allowed by the Universal Treatment Standards (UTS) applicable for this waste, namely 40 CFR (Code of Federal Regulations) 268.48. On the contrary, mercury concentration in the leachates related to the solidified alkali-activated mixtures is much below the standard limit even for those mixtures containing a high percentage of waste glass. For the blank mixtures (mixtures without waste glass) and for those with just five percentages of waste glass, the concentration of mercury is below the detection limit. All these results suggest a very good potential of the alkali-activated materials to immobilize mercury which is the hazardous component of these waste.

Compressive strength test results for the five different alkali-activated materials, presented in Fig. 2, suggest that the increasing addition of the waste glass does not lead to the obtaining of some weak materials. However, it seems that the addition of waste glass in a small proportion to the

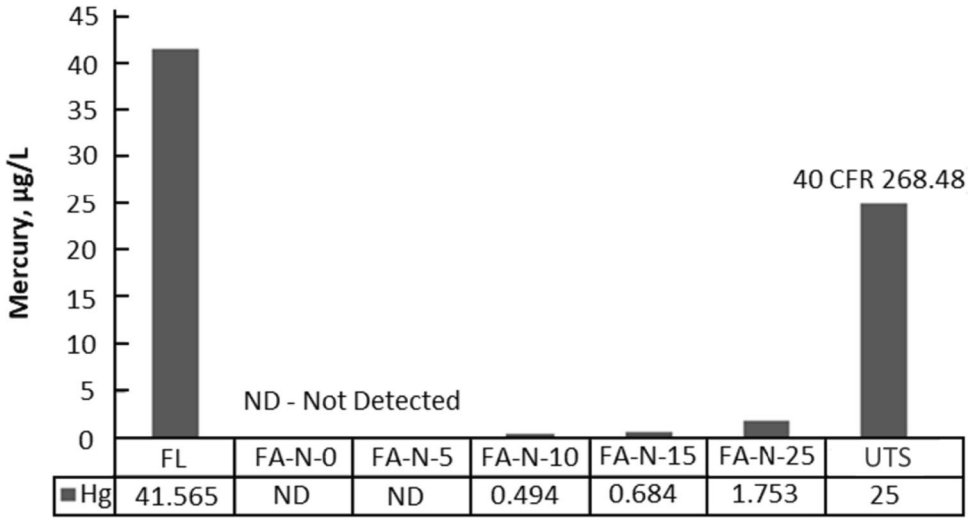

Fig. 1 TCLP results (UTS—non-wastewater standard, mercury—all others: 0.025 mg/l TCLP)

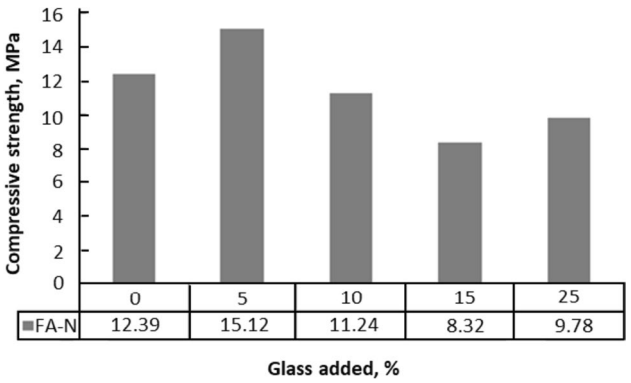

Fig. 2 Influence of the waste glass addition on the compressive strength of the alkali-activated materials

mixture has a beneficial effect on the mechanical properties of the alkali-activated materials. The addition of increasingly larger waste glass weakens the material, but not in such a great extent compared to the best-obtained results. This mechanical behavior suggests the active nature of the waste glass, which is involved in the polycondensation processes that occur during the alkali activation of the raw materials. However, according to the ASTM C90-16a standard, the mixtures FA-N-0 and FA-N-5 meet the requirements regarding their compressive strength (must be higher than 12.4 MPa) and therefore can be used for the manufacture of loadbearing concrete masonry units. Because the content of alumina in the waste glass is very low compared with its content in silica, the increasing addition of the waste glass powder to the synthesis mixture dramatically disturbs the SiO_2/Al_2O_3 initial molar ratio (from approximately 4.8, corresponding to the mixture with 5% waste glass, to approximately 6.9, corresponding to the mixture with 25% waste glass). The aluminosilicate gel depends on a certain minimum value of the amount of reactive alumina that should exist in the reaction mixture. In this respect, for high SiO_2/Al_2O_3 molar ratio, it is expected that the rate at which silica from the raw material is dissolved decreases as the reaction time increases and the amount of alumina (much more reactive than silica in alkaline environment) decreases in the reaction mixture (Fernández-Jiménez et al. 2006; Davidovits 2020). This results in the increase of the unreacted glassy mass fraction that could be associated with the defect sites which negatively affect the mechanical performances of the alkali-activated material (Duxson et al. 2007).

Considering all the results presented above, it seems that both leaching and mechanical behavior of the alkali-activated materials is much influenced by their mineralogical and microstructural characteristics as well as by the initial characteristics of the raw materials. As shown in Fig. 3A, the fly ash particles are consisting mainly of compacted spheres of different size (points 1), some irregularly shaped particles (points 2) probably consisting of unburnt coal and other thronged mineral particles (Pedraza et al. 2015; Xing et al. 2019). The electron micrograph of the waste glass powder (Fig. 3B) shows a medley distribution of particles with irregular and smooth shapes of different size (points 3).

Comparative to the micrographs of the unreacted materials, ones of alkali-activated mixtures (FA-N-0 and FA-N-10) highlight the presence of the alkali aluminosilicate gels well as the presence of the partially or unreacted fly ash and waste glass particles. In this respect, from the micrographs of FA-N-0 mixture (Fig. 3C and E) it can be seen that among of some unreacted spheres (points 4) there is an amorphous alkali aluminosilicate gel (points 5). However, the considerable amount of partially or unreacted spheres (Fig. 3C) indicates a moderate polycondensation degree of the synthesis mixture.

In addition, the micrographs presented in Fig. 3D (corresponding to the FA-N-10 mixture) that also suggest a moderate reacted mixture, it can be seen the presence of

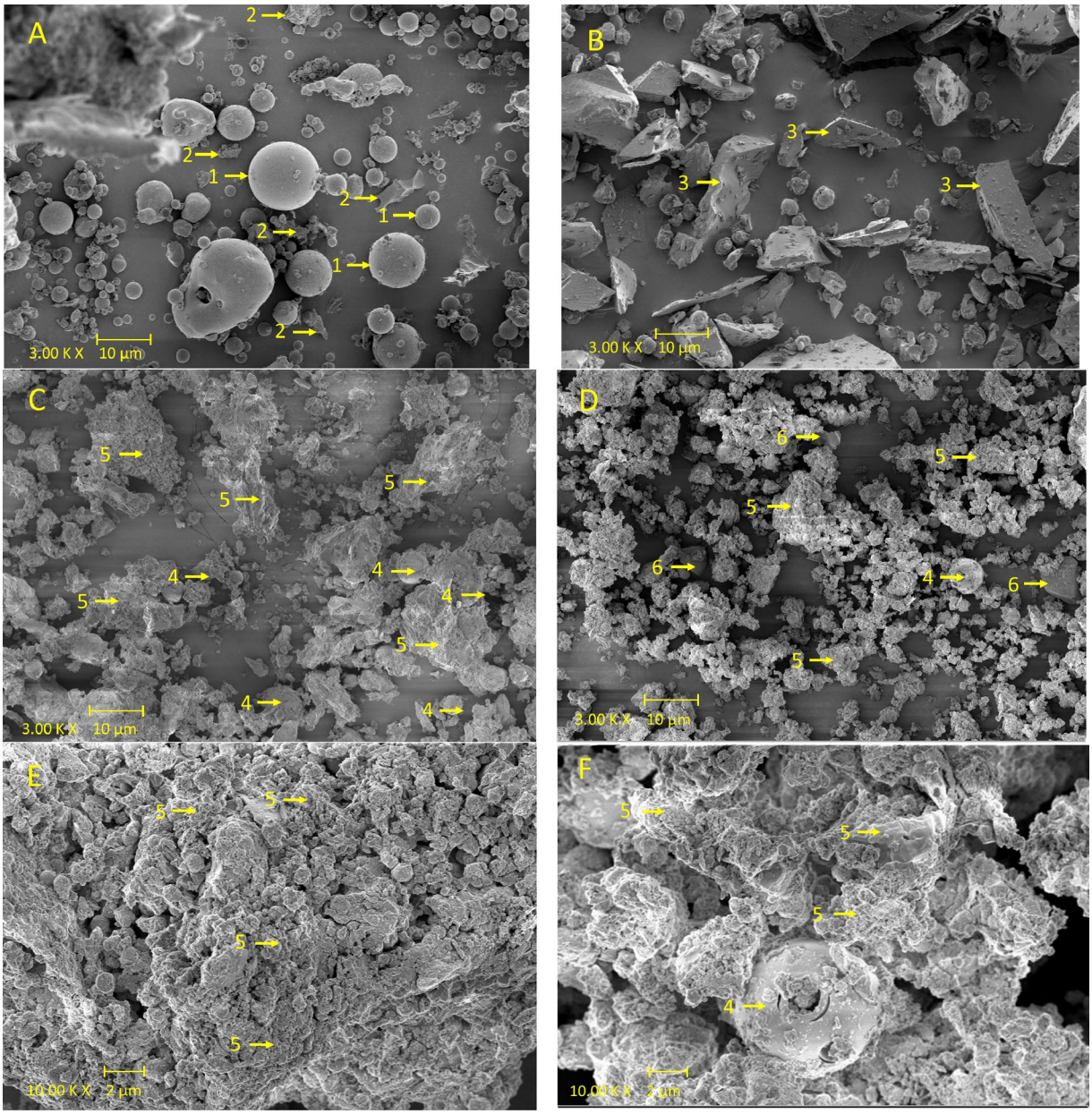

Fig. 3 Electron micrographs of raw materials and of two alkali-activated mixtures: **A** fly ash; **B** waste glass; **C** and **E** FA-N-0 mixture; **D** and **F** FA-N-10 mixture

some unreacted waste glass particles (points 6) among of partially or unreacted fly ash spheres (point 4). Contrary to the unreacted fly ash spheres (Fig. 3D), these unreacted waste glass particles still have a smooth surface indicating a poor adherence with the alkali aluminosilicate gel framework. The weak adhesion of the unreacted glass particles to the alkali aluminosilicate gel framework confers a low mechanical resistance, a fact demonstrated by the results of the compression strength tests (Fig. 2). Comparing the last two micrographs presented in Fig. 3 (Fig. 3E and F), it seems the morphology of the two mixtures is different. In the case of FA-N-0 mixture (Fig. 3E) the morphology of the reacted mixture indicates some continuity, most likely due to the formation of the alkali aluminosilicate gel that confers good adhesion between partially reacted or unreacted fly ash particles. On the contrary, in the case of FA-N-10 mixture (Fig. 3F) this continuity seems to be ensured by the presence of a continuous polycondensed phase, most likely due to the formation of a significant amount of silicate gel during the alkaline activation of the added waste glass. However, it appears that between these covered zones there are some relatively big gaps that could be attributable to the poor

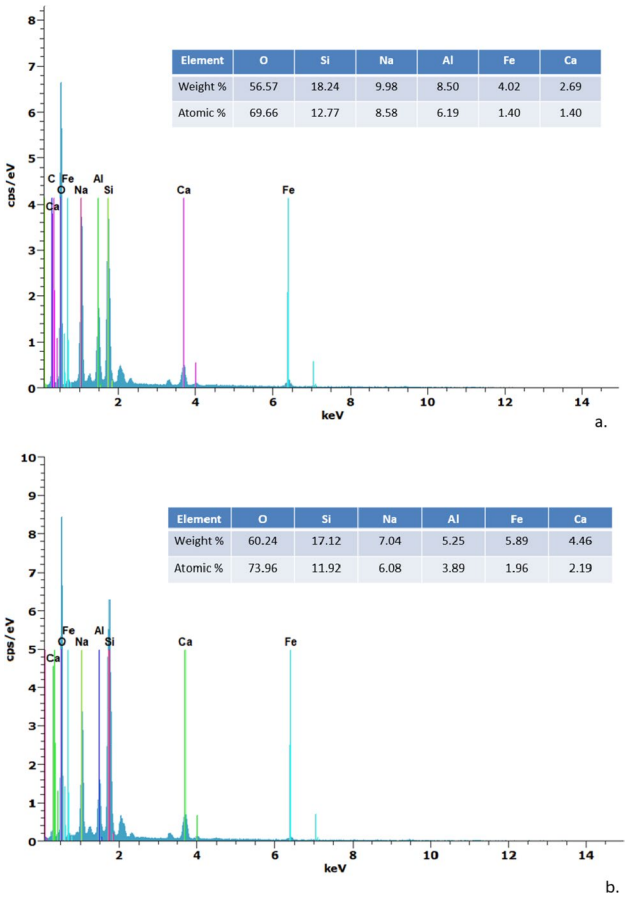

Fig. 4 EDX spectra of two alkali-activated mixtures: **A** FA-N-0 mixture; **B** FA-N-10 mixture

adhesion between the alkali aluminosilicate gel framework and the smooth surface of the waste glass particles.

EDX analysis (performed for specific spots of the SEM images) of the two types of alkali-activated materials (Fig. 4) indicated a Si/Al ratio of 2.14 for FA-N-0 and 3.26 for FA-N-10, as well as a Na/Al ratio of 1.17 for FA-N-0 and 1.34 for FA-N-10. Alkali-activated materials that have a Si/Al molar ratio in the range of 1–3 and a Na/Al molar ratio close to unity are mainly formed by silico-aluminates with Si^{4+} and Al^{3+} in fourfold coordination thus forming continuous well-joined sodium aluminosilicate hydrate (N-A-S-H) gels (Baskar et al. 2023). High values of the Si/Al ratio are often associated with the unreacted glassy fraction of the alkali-activated mixture that acts as defect sites with a negative effect on its mechanical properties (Duxson et al. 2007). These results are in agreement with those obtained from compressive strength tests and SEM analysis.

To get more information on the pore structure of the alkali-activated materials, the nitrogen adsorption–desorption isotherms were measured for both raw materials and alkali-activated materials. These are presented in Fig. 5. As can be seen, these isotherms appear to be of type II (b), having a hysteresis loop of type H3 specific to mesoporous materials (Rouquerol et al. 2014). The pore size distribution calculated using the BJH method, which is also presented in Fig. 5, reveals that most of the pores of all the materials have a diameter around of 3.8 nm, with a visible extending trend to higher values in the case of FA-N-10 mixture. The major difference which was registered is between their total pore volume as well as their surface area. In this respect, the total pore volume for FA-N-0 mixture is 1.403×10^{-2} cm^3/g while for FA-N-10 mixture is 7.459×10^{-2} cm^3/g. The BET surface area for FA-N-0 mixture is 7.834 m^2/g while for FA-N-10 mixture is 12.55 m^2/g (an almost two times more porous system). These results show an important difference between the two alkali-activated systems in terms of their microstructural characteristics and, in this respect, support the results obtained from compressive strength tests and SEM–EDX analysis.

The results obtained by XRD analysis (Fig. 6) show that the raw materials (patterns 1 and 2) are basically constituted from (amorphous) vitreous phase with just some minor crystalline phases. These are quartz (Q), mullite (M), hematite (H) and gypsum (G) for fly ash, and hydroxyapatite (A) for waste glass. The hydroxyapatite in waste glass derived from "phosphorus" which is the fluorescent powder used in fluorescent lamps manufacture. The patterns 3 and 4 corresponding to the two types of alkali-activated materials also highlight the low crystalline structure of these materials that is associated with the formation of the silicate and aluminosilicate gels. However, comparing these patterns with those of raw materials it can be seen that the crystalline phases initially present in the raw materials were not much altered during the activation reactions, except for gypsum in the fly ash and hydroxyapatite in the waste glass. In addition, two other crystalline phases were identified in the two alkali-activated systems, namely the zeolites hydroxysodalite (HS) and cancrinite (C).

Conclusions

The aim of this work was to explore the feasibility of using the waste glass containing mercury, which comes from discarded fluorescent lamps, as active precursor in the fly ash-based alkali-activated systems. The main findings are as follows:

1. The alkali-activated materials based on fly ash and powdered waste glass have a high potential to immobilize mercury, which is the major hazardous component of the waste glass used. Thus, it was highlighted that the concentration of mercury in the leachate corresponding to the synthesis mixture with the largest addition of used

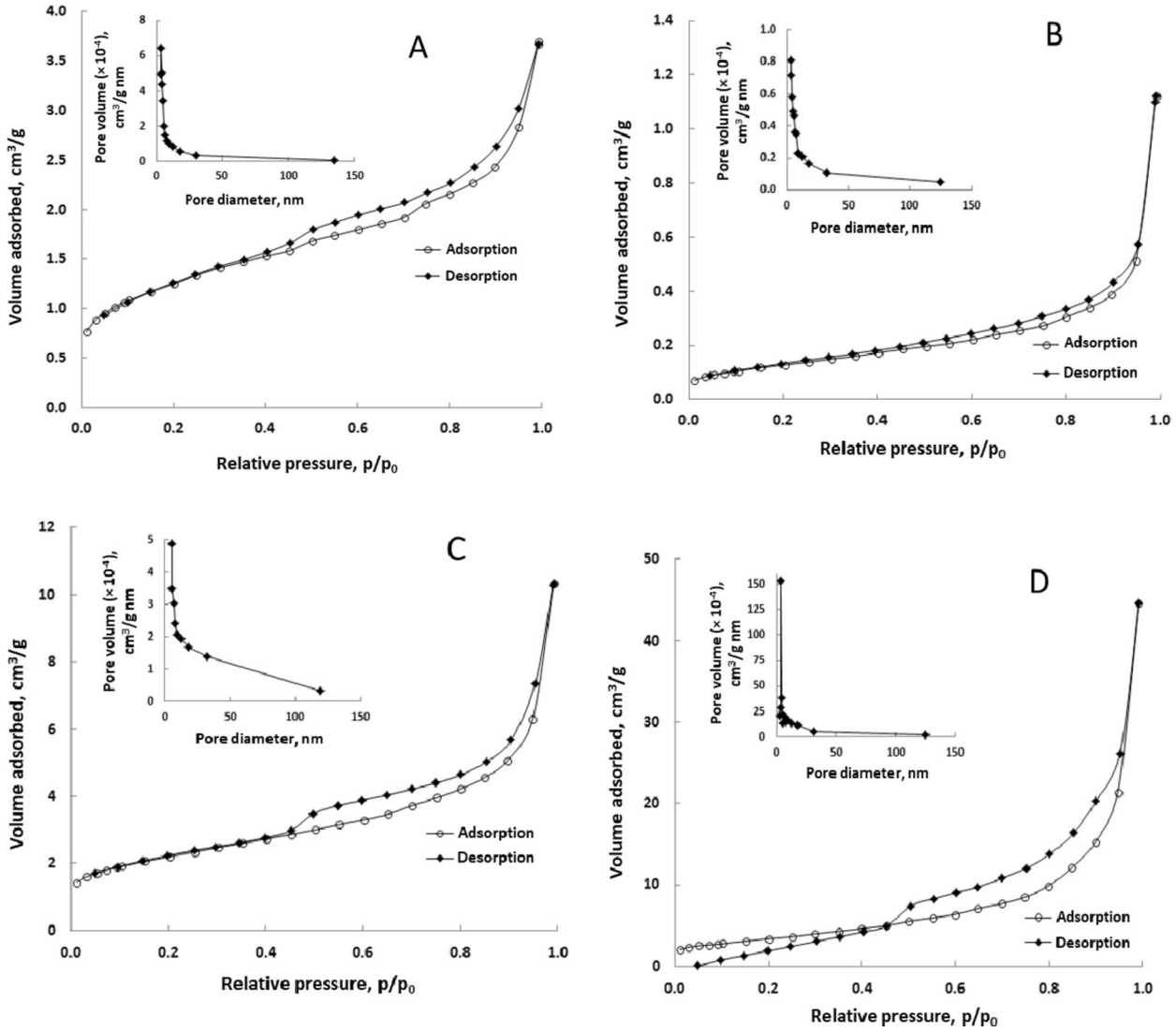

Fig. 5 N_2 adsorption–desorption isotherms and pore size distribution of both raw materials and alkali-activated materials: **A** fly ash; **B** waste glass; **C** FA-N-0 mixture; **D** FA-N-10 mixture

glass is approximately 14 times lower than the maximum limit imposed by the leaching standard.

2. The addition of the waste glass to the alkali-activated system leads to some changes regarding the mechanical performances of the final products, and it seems that these changes are dependent on the amount of waste glass added. The best result in terms of compressive strength was obtained for the synthesis mixture to which 5% by mass of glass waste was added (FA-N-5), for which a value of over 15 MPa was recorded, which recommends it, according to the standards, to be used for the manufacture of loadbearing concrete masonry units.
3. The addition of the waste glass to the alkali-activated system results in some important microstructural changes such as the increase of the alkali-activated materials porosity. Thus, the total pore volume is more than five times higher, and the specific BET surface is approximately two times higher in the case of the FA-N-10 mixture compared to the FA-N-0 mixture.
4. The increasing addition of waste glass by more than 5% of the total mass of the synthesis mixture leads to the increase of the unreacted glassy fraction in the alkali-activated materials. The unreacted glassy fraction can be associated with the appearance of some defect sites which in turn lead to a decrease in the mechanical performance of alkali-activated materials.

Therefore, it can be concluded that the adding appropriate amounts of waste glass to the fly ash-based alkali-activated mixture leads to obtaining alkali-activated materials with

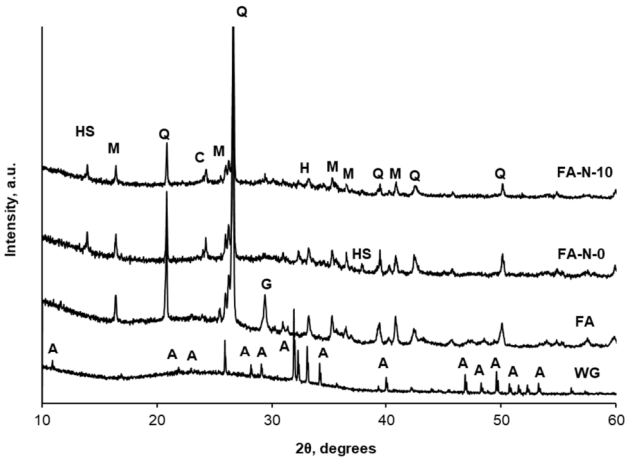

Fig. 6 XRD patterns of raw materials and alkali-activated materials; Q–quartz (JCPDS Card 33–1161), H–hematite (JCPDS Card 84–0311), M–mullite (JCPDS Card 15–0776), G–gypsum (JCPDS Card 74–1433), A–hydroxyapatite (JCPDS Card 09–0432), HS–hydroxysodalite (JCPDS Card 11–0401), C–cancrinite (JCPDS Card 73–0540)

good mechanical properties and with a high potential to immobilize the mercury, which is the main hazardous constituent of the waste glass used.

Author contributions All authors contributed to the study conception and design. Material preparation, data collection and analysis were performed by Nicolae Marin, Liliana Bobirică and, Luoana Florentina Pascu. The first draft of the manuscript was written by Constantin Bobirică and Cristina Orbeci. All authors commented on previous versions of the manuscript. All authors read and approved the final manuscript.

Funding This work has been funded by the European Social Fund from the Sectoral Operational Programme Human Capital 2014–2020, through the Financial Agreement with the title "Training of PhD students and postdoctoral researchers in order to acquire applied research skills—SMART", Contract No. 13530/16.06.2022-SMIS code: 153734.

Data availability The datasets generated during and/or analyzed during the current study are not publicly available due to the policy adopted by our department but are available from the corresponding author on reasonable request.

Declarations

Competing interests The authors declare no competing interests.

References

Abbas S (2023) Preventive measures of alkali-silica reaction in concrete buildings: use of hybrid waste coal ash and steel wire cut fibers. Buildings 13:710. https://doi.org/10.3390/buildings13030710

Baskar P, Annadurai S, Sekar K, Prabakaran M (2023) A review on fresh, hardened, and microstructural properties of fibre-reinforced geopolymer concrete. Polymers 15:1484. https://doi.org/10.3390/polym15061484

Çelik Aİ, Tunç U, Bahrami A, Karalar M, Mydin MAO, Alomayri T, Özkılıç YO (2023) Use of waste glass powder toward more sustainable geopolymer concrete. J Mater Res Technol 24:8533–8546. https://doi.org/10.1016/j.jmrt.2023.05.094

Davidovits J (2020) Geopolymer Chemistry and Applications. Institut Géopolymère, France

Duxson P, Fernández-Jiménez A, Provis JL, Lukey GC, Palomo A, van Deventer JSJ (2007) Geopolymer technology: the current state of the art. J Mater Sci 42:2917–2933. https://doi.org/10.1007/s10853-006-0637-z

Epa US (1997) Mercury emissions from the disposal of fluorescent lamps, Final Report. Office of Solid Waste, Environmental Protection Agency, USA

Fernández-Jiménez A, Palomo A, Sobrados I, Sanz J (2006) The role played by the reactive alumina content in the alkaline activation of fly ashes. Micropor Mesopor Mat 91:111–119. https://doi.org/10.1016/j.micromeso.2005.11.015

Frasson BJ, Rocha JC (2023) Reaction mechanism and mechanical properties of geopolymer based on kaolinitic coal tailings. Appl Clay Sci 233:106826. https://doi.org/10.1016/j.clay.2023.106826

Hama SM, Ali ZM, Zayan HS, Mahmoud AS (2023) Structural behavior of reinforced concrete incorporating glass waste as coarse aggregate. J Struct Integr Maint 8:59–66. https://doi.org/10.1080/24705314.2023.2165470

Komnitsas K, Zaharaki D (2007) Geopolymerization: a review and prospects for the minerals industry. Miner Eng 20:1261–1277. https://doi.org/10.1016/j.mineng.2007.07.011

Lei J, Fu J, Yang E-H (2020) Alkali-silica reaction resistance and pore solution composition of low-calcium fly ash-based geopolymer concrete. Infrastructures 5:96. https://doi.org/10.3390/infrastructures5110096

Li T, Meng F, Yang J, Li H (2023) Identification of mercury species in spent fluorescent lamps and mercury recovery by distillation. Energy Rep 9:64–72. https://doi.org/10.1016/j.egyr.2023.04.025

Liu Z, Shi C, Shi Q, Tan X, Meng W (2022) Recycling waste glass aggregate in concrete: mitigation of alkali-silica reaction (ASR) by carbonation curing. J Clean Prod 370:133545. https://doi.org/10.1016/j.jclepro.2022.133545

Long W-J, Lin C, Ye T-H, Dong B, Xing F (2021) Stabilization/solidification of hazardous lead glass by geopolymers. Constr Build Mater 294:123574. https://doi.org/10.1016/j.conbuildmat.2021.123574

Occhicone A, Vukčević M, Bosković I, Mingione S, Ferone C (2022) Alkali-activated red mud and construction and demolition waste-based components: characterization and environmental assessment. Materials 15:1617. https://doi.org/10.3390/ma15041617

Özkılıç YO, Çelik Aİ, Tunç U, Karalar M, Deifalla A, Alomayri T, Althoey F (2023) The use of crushed recycled glass for alkali activated fly ash based geopolymer concrete and prediction of its capacity. J Mater Res Technol 24:8267–8281. https://doi.org/10.1016/j.jmrt.2023.05.079

Pedraza SP, Pineda Y, Gutiérrez O (2015) Influence of the unburned residues in fly ash additives on the mechanical properties of cement mortars. Procedia Mater Sci 9:496–503. https://doi.org/10.1016/j.mspro.2015.05.022

Rey-Raap N, Gallardo A (2012) Determination of mercury distribution inside spent fluorescent lamps by atomic absorption spectrometry. Waste Manag 32:944–948. https://doi.org/10.1016/j.wasman.2011.12.001

Ricciotti L, Occhicone A, Ferone C, Cioffi R, Roviello G (2023) Ecodesign of geopolymer-based materials recycling porcelain stoneware wastes: a life cycle assessment study. Environ Dev Sustain. https://doi.org/10.1007/s10668-022-02870-x

Rouquerol F, Rouquerol J, Sing KSW, Llewellyn P, Maurin G (2014) Adsorption by Powders and Porous Solids. Academic Press, London

Tian Q, Bai Y, Pan Y, Chen C, Yao S, Sasaki K, Zhang H (2022) Application of geopolymer in stabilization/solidification of hazardous pollutants: a review. Molecules 27:4570. https://doi.org/10.3390/molecules27144570

Xing Y, Guo F, Xu M, Gui X, Li H, Li G, Xia Y, Han H (2019) Separation of unburned carbon from coal fly ash: a review. Powder Technol 353:372–384. https://doi.org/10.1016/j.powtec.2019.05.037

Zhang J, Provis JL, Feng D, van Devente JSJ (2008) Geopolymers for immobilization of Cr^{6+}, Cd^{2+}, and Pb^{2+}. J Hazard Mater 157:587–598. https://doi.org/10.1016/j.jhazmat.2008.01.053

Authors and Affiliations

Nicolaie Marin[1] · Cristina Orbeci[1] · Liliana Bobirică[1] · Luoana Florentina Pascu[2] · Constantin Bobirică[1]

✉ Constantin Bobirică
constantin.bobirica@upb.com

[1] Department of Analytical Chemistry and Environmental Engineering, National University of Science and Technology Politehnica of Bucharest, 1-7 Polizu, 011061 Bucharest, Romania

[2] National Research and Development Institute for Industrial Ecology, 57-73 Drumul Podu Dâmboviţei, 060652 Bucharest, Romania